Low-Dimensional Sulfoantimonates with Metal Complexes as Counterions. Hydrothermal Synthesis and Properties of $[M(en)_3]Sb_2S_4$ (M = Co, Ni) and $[M(en)_3]Sb_4S_7$ (M = Fe, Ni)

Hans-Oscar Stephan and Mercouri G. Kanatzidis*

Department of Chemistry and Center for Fundamental Materials Research, Michigan State University, East Lansing, Michigan 48824

Received May 22, 1997[⊗]

$[M(en)_3]Sb_2S_4$ (M = Co, Ni) and $[M(en)_3]Sb_4S_7$ (M = Fe, Ni) were prepared from the MX_2/Na_3SbS_3/en system (X = Cl, Br; en = ethylenediamine) under hydrothermal conditions. Orange-yellow $[Ni(en)_3]Sb_2S_4$ (**1**) crystallizes in the monoclinic space group $P2_1/c$ (No. 14) with $a = 10.538(2)$ Å, $b = 14.460(4)$ Å, $c = 12.434(5)$ Å, $\beta = 99.93(2)°$, and $Z = 4$. Green-yellow $[Co(en)_3]Sb_2S_4$ (**2**) crystallizes as a superstructure of **1** with $a = 21.131(4)$ Å, $b = 14.619(2)$ Å, $c = 12.540(2)$ Å, $\beta = 100.50(1)°$, and $Z = 8$. The antimony sulfide frameworks in **1** and **2** consist of SbS_3 pyramids sharing two corners to form $1/\infty[SbS_2]^-$ chains. Orange-yellow $[Ni(en)_3]Sb_4S_7$ (**3**) crystallizes in the monoclinic space group $P2_1/c$ (No. 14) with $a = 9.930(1)$ Å, $b = 14.212(2)$ Å, $c = 17.242(2)$ Å, $\beta = 102.55(1)°$, and $Z = 4$. The $1/\infty[Sb_4S_7]^{2-}$ chains are formed by corner-sharing SbS_3 units. Three of these pyramids are arranged to cyclic Sb_3S_6 trimers which share two of the three exocyclic S-atoms with the fourth SbS_3 units to form infinite chains. $[Fe(en)_3]Sb_4S_7$ (**4**) is isostructural to **3**. In all four compounds the tris(ethylenediamine)metal(II) complexes act as counterions. The thermal, magnetic and optical properties of compounds **1**−**4** are reported.

Introduction

Ternary antimony(III) sulfide compounds are accessible primarily via three synthetic methods. The first is the direct combination of binary sulfides A_2S/Sb_2S_3 (A = Na, K, Rb, Cs) and $(AE)S/Sb_2S_3$ (AE = Ca, Sr, Ba) at high temperature gives $ASbS_2$[1] (A = Na, K, Rb, Cs), $Ca_2Sb_2S_5$,[2] $Ba_8Sb_6S_{17}$,[3] and $Sr_3Sb_4S_9$,[4] while flux reactions of Sb in CsS_x melts gives $Cs_2Sb_4S_8$[5] and $CsSbS_6$.[5] The third method involves hydro(solvo)thermal conditions and is well suited not only for strictly inorganic materials such as $Cs_3Sb_5S_9$,[6] *a*,*b*-$Rb_2Sb_4S_7$,[7] $Cs_6Sb_{10}S_{18}\cdot 1.2H_2O$,[8] $K_2Sb_4S_7\cdot H_2O$,[9] $K_2Sb_4S_7$,[10] $Tl_2Sb_3S_5$,[11] $Cs_3Ag_2Sb_3S_8$,[12] and α,*β*-Cs_2AgSbS_4[12] but also for open Sb/S frameworks in which the void space is filled with organic cations. Examples include $[Me_4N]Sb_3S_5$,[13] $[(C_3H_7)_4N]Sb_3S_5$,[14] $[N_2C_4H_8]Sb_4S_7$,[14] $[MeNH_3]_2Sb_8S_{13}$,[15] and $Cs_5Sb_8S_{18}$.[16]

In recent reports, we have shown that hydrothermal reactions of molecular $[AsS_3]^{3-}$ ions with M^{n+} ions in the presence of organic cations yield novel materials in which higher aggregated $[As_xS_y]^{n-}$ units are connected with the metal ions to form one-dimensional ($[Ph_4P]_2Hg_2As_4S_9$[17] and $[Ph_4P]_2InAs_3S_7$[18]) or two-dimensional ($[Me_4N]HgAs_3S_6$[17] and $[Me_4N]_2[Rb]BiAs_6S_{12}$[18]) structures. In order to learn more about the analogous antimony system, we started to explore the system M^{n+}/SbS_3^{3-}/en (en = ethylenediamine) with the goal being to synthesize open-framework materials containing (thermally decomposable) enH^+ or enH_2^{2+} ions. In these studies, we discovered the compound $[Co(en)_3]CoSb_4S_8$[19] in which porous $CoSb_4S_8^{2-}$ layers are surrounded by *in-situ* generated $[Co(en)_3]^{2+}$ cations. Here we report on $[M(en)_3]Sb_2S_4$ (M = Co, Ni) and $[M(en)_3]Sb_4S_7$ (M = Fe, Ni), two new compounds in which binary Sb/S chains are separated by paramagnetic $[M(en)_3]^{2+}$ cations.

Experimental Section

Reagents. Chemicals were used as obtained: (i) antimony powder, 99.999+% purity, −200 mesh, Cerac Inc., Milwaukee, WI; (ii) sulfur powder, sublimed, J. T. Baker Chemical Co., Phillipsburg, NJ; (iii) sodium metal, chunks, Fluka Chemie AG, Buchs, Switzerland; (iv) methanol, anhydrous, Malinckrodt Inc., Paris, KY; (v) diethyl ether, ACS anhydrous, EM Science, Inc., Gibbstown, NJ.

Syntheses. All manipulations were carried out under dry nitrogen atmosphere in a Vacuum Atmosphere Dri-Lab glovebox. Na_2S was prepared by reduction of sulfur with sodium in liquid ammonia.[20] For the preparation of Na_3SbS_3, we used a modified literature procedure.[21] Na_2S, Sb, and S were mixed carefully in a 1.5/1/1.5 molar ratio and loaded into a pyrex tube. The tube was sealed under high vacuum (4.0×10^{-4} mbar), slowly heated to 550 °C and isothermed at this temperature for 85 h. After cooling (20 deg/h), yellow-brown Na_3SbS_3 was isolated as a pure phase.

$[Ni(en)_3]Sb_2S_4$ (1). $NiCl_2$ (130 mg; 1 mmol) and Na_3SbS_3 (574 mg; 2 mmol) were carefully mixed and loaded into a teflon-lined digestion bomb (~20 mL). A deoxygenated mixture of 2.2 mL of water and

[⊗] Abstract published in *Advance ACS Abstracts,* December 1, 1997.

(1) (a) Olivier-Fourcade, E.; Phillippot, J.; Maurin, M. *Z. Anorg. Allg. Chem.* **1978**, *446*, 159. (b) Graf, H. A.; Schäfer, H. *Z. Anorg. Allg. Chem.* **1975**, *414*, 210. (c) Kanishcheva, A. S.; Kuznetsov, V. G.; Lazarev, V. B.; Tarasova, T. G. *Zh. Strukt. Khim.* **1977**, *18*, 1069. (d) Kanishcheva, A. S.; Mikhailov, Y. N.; Kuznetsov, V. G.; Batog, V. N. *Dokl. Akad. Nauk SSR* **1980**, *251*, 603.
(2) Cordier, G.; Schäfer, H. *Rev. Chim. Miner.* **1981**, *18*, 218.
(3) Dorrscheidt, W.; Schäfer, H. *Z. Naturforsch.* **1981**, *36B*, 410.
(4) Cordier, G.; Schwidetzky, C.; Schäfer, H. *Rev. Chim. Miner.* **1982**, *19*, 179.
(5) McCarthy, T. J.; Kanatzidis, M. G. *Inorg. Chem.* **1994**, *33*, 1205.
(6) Sheldrick, W. S.; Häusler, H.-J. *Z. Anorg. Allg. Chem.* **1988**, *561*, 149.
(7) (a) Dittmar, V. G.; Schäfer, H. *Z. Anorg. Allg. Chem.* **1978**, *441*, 93. (b) Sheldrick, W. S.; Häusler, H.-J. *Z. Anorg. Allg. Chem.* **1988**, *557*, 105.
(8) Parise, J. B. *J. Chem. Soc., Chem. Commun.* **1990**, *22*, 1553.
(9) Eisenmann, B.; Schäfer, H. *Z. Naturforsch.* **1979**, *34b*, 383.
(10) Graf, H. A.; Schäfer, H. *Z. Naturforsch.* **1972**, *27b*, 735.
(11) Gostojic, M.; Nowacki, W.; Engle, P. *Z. Kristallogr.* **1982**, *159*, 217.
(12) Wood, P. T.; Schimek, G. L.; Kolis, J. W. *Chem. Mater.* **1996**, *8*, 721.
(13) Parise, J. B. *Science* **1991**, *251*, 293.
(14) Parise, J. B.; Ko, Y. *Chem. Mater.* **1992**, *4*, 1446.
(15) Wang, X.; Liebau, F. *J. Solid State Chem.* **1994**, *111*, 385.
(16) Schimek, G. L.; Kolis, J. W. *Inorg. Chem.* **1997**, *36*, 1689.
(17) Chou, J.-H.; Kanatzidis, M. G. *Chem. Mater.* **1995**, *7*, 5.
(18) Chou. J.-H.; Kanatzidis, M. G. *Inorg. Chem.* **1994**, *33*, 1001.
(19) Stephan, H.-O.; Kanatzidis, M. G. *J. Am. Chem. Soc.* **1996**, *118*, 12226.
(20) Fehér, F. In *Handbuch der präparativen Anorganischen Chemie Band 1*; Brauer, G., Ed.; Ferdinand Enke Verlag: Stuttgart, Germany, 1975; p 372.
(21) Sommer, H.; Hoppe, R. *Z. Anorg. Allg. Chem.* **1977**, *430*, 199.

S0020-1669(97)00609-5 CCC: $14.00

0.8 mL of ethylenediamine (12 mmol) was added. The container was closed and exposed to 130 °C for 4 days. The product was isolated by washing with water and then methanol and ether, giving orange cube-like crystals and some undesired black powder, a mixture of Sb_2S_3 and $NaSbS_2$. In a subsequent purification step, this crude material was submerged in water and sonicated for a few minutes. Most of the black powder was suspended in water and was decanted, leaving behind the pure compound. This procedure was repeated until the water remained clear. Yield: 275 mg (0.45 mmol; 45%). Quantitative microprobe analysis on the single crystals gave $Ni_{1.0}Sb_{1.2}S_{2.5}$ (average of three data aquisitions). Far-IR spectroscopy (CsI matrix) gave 10 absorbances at 525 (m), 517 (m), 490 (m), 397 (s), 378 (m), 367 (m), 328 (w), 308 (m), 303 (m), and 269 cm^{-1} (s). Raman spectroscopy gave 5 signals at 388 (s), 365 (m), 309 (s), 262 (m), and 169 cm^{-1} (w).

$[Co(en)_3]Sb_2S_4$ (2). $CoBr_2$ (176 mg; 0.8 mmol) and Na_3SbS_3 (184 mg; 0.64 mmol) were carefully mixed and loaded into a teflon-lined digestion bomb. A deoxygenated mixture of 2.6 mL of water and 1.92 mL of ethylenediamine (28.8 mmol) was added. The rest of the procedure is identical to the one described above. An amount of 25 mg (0.08 mmol; yield 13% based on Sb) of yellow-green cubes was obtained. Far-IR spectroscopy (CsI matrix) gave 10 absorbances at 528 (w), 520 (m), 495 (w), 401 (s), 372 (w), 358 (w), 330 (w), 311 (m), 307 (m), and 272 cm^{-1} (s).

$[Ni(en)_3]Sb_4S_7$ (3). $NiCl_2$ (130 mg; 1 mmol) and Na_3SbS_3 (430 mg; 1.5 mmol) were carefully mixed and loaded into a digestion bomb. A deoxygenated mixture of 2.6 mL of water and 0.4 mL of ethylenediamine (6 mmol) was added. The container was closed and exposed to 130 °C for 4 days. The material was isolated in water and washed with methanol and ether. Orange chunky crystals were obtained along with some undesired black powder, which was removed according to the procedure described above. Yield: 150 mg (0.15 mmol; 42% based on Sb). If the reaction is allowed to proceed for 3 weeks, the material can be obtained as very large crystals with egde lengths of up to 10 mm. Quantitative microprobe analysis on the single crystals gave $Ni_{1.0}Sb_{3.2}S_{6.5}$ (average of four data aquisitions). Far-IR (CsI matrix) gave 9 absorbances at 506 (w), 496 (w), 487 (w), 384 (s), 354 (s), 321 (s), 293 (s), 282 (s), and 259 cm^{-1} (s). Raman spectroscopy gave 4 signals at 379 (w), 326 (s), 281 (w), and 160 (s) cm^{-1}.

$[Fe(en)_3][Sb_4S_7]$ (4). $FeCl_2$ (104 mg; 0.8 mmol) and Na_3SbS_3 (253 mg; 0.88 mmol) were carefully mixed and loaded into a teflon-lined digestion bomb. A deoxygenated mixture of 1.8 mL of water and 0.64 mL of ethylenediamin (9.6 mmol) was added. The container was closed and exposed to 130 °C for 4 days. The rest of the procedure is identical to the one described above. Yield: 50 mg (0.05 mmol; 24% based on Sb), yellow crystals. Quantitative microprobe analysis on the single crystals gave $Fe_{1.0}Sb_{3.5}S_{6.9}$ (average of four data aquisitions). Far-IR (CsI matrix) gave 7 absorbances at 476 (b), 384 (s), 354 (s), 320 (m), 293 (m), 283 (m), and 259 cm^{-1} (s). Raman spectroscopy gave two signals at 326 (s) and 180 (m) cm^{-1}.

Physical Measurements. FT-IR spectra of compounds **1**−**4** were recorded as solids in a CsI matrix. The samples were ground with dry CsI into a fine powder and pressed into translucent pellets. The spectra were recorded in the far IR region (100−600 cm^{-1}; resolution, 4 cm^{-1}) with a Nicolet Magna-IR 750 Spectrometer, Series II. Raman spectra were recorded with a Biorad FT-Raman spectrometer. Quantitative microprobe analyses of the compounds were performed with a JEOL JSM-6400V scanning electron microscope (SEM) equipped with a Tracor Northern energy dispersive spectroscopy (EDS) detector. Data aquisition was performed with an acceleration voltage of 20 kV and a 1 min accumulation time.

Single crystal UV/vis spectra were recorded on a computer-controlled Hitachi FT Spectrophotometer U 6000 associated with an Olympus BH2-UMA Microscope in the wavelength range of 380−900 nm. Optical diffuse reflectance measurements were performed at room temperature with a Shimadzu UV-31-1 PC double-beam, double monochromator spectrophotometer operating in the 200−2500 nm region. The instrument was equipped with an integrating sphere and controlled by a personal computer. The measurement of diffuse reflectivity can be used to obtain values for the band gap which agree well with values obtained by absorption measurements on single crystals of the same material. The digitized spectra were processed using the Kaleidagraph software program. $BaSO_4$ powder was used as reference (100% reflectance). Absorption data were calculated from the reflectance data using the Kubelka−Munk[22] function:

$$\alpha/S = (1 - R)^2/2R$$

R is the reflectance at a given wavelength, α is the absorption coefficient, and S is the scattering coefficient. The scattering coefficient has been shown to be virtually wavelength independent for particles larger than 5 mm, which is smaller than the particle size of the samples used here.

Thermogravimetric analyses (TGA) were performed with a computer-controlled Shimadzu TGA-50 thermal analyzer. The ground single crystals (~10 mg total mass) were loaded into quartz baskets and heated and cooled with 2 °C/min under a nitrogen stream of 46 mL/min. The samples were heated to 500 °C. The TGA samples were examined by powder X-ray diffraction (XRD) after the experiment.

Variable temperature magnetic susceptibility measurements were performed using a MPMS Quantum Design SQUID magnetometer between 2 and 300 K. Single crystals were ground to a fine powder to minimize anisotropic effects. The powder was loaded into a polyethylene bag and sealed. The applied magnetic field was 2000 G. Corrections for diamagnetism for both the sample and the bag were applied.

Crystallographic Studies. All compounds were examined by XRD for the purpose of phase purity and identification with a Rigaku rotating anode (Cu K_α) X-ray powder diffractometer, Rigaku-Denki/RW400F2 (Rotaflex), operating at 45 kV and 100 mA.

Single crystal X-ray diffraction data for **1**−**3** were collected on a Rigaku AFC6 diffractometer and the $\omega/2\theta$ scan technique was used. None of the crystals showed any significant intensity decay as judged by three check reflections measured every 150 reflections throughout the data collection. Unique data sets were collected in all cases. The $2\theta_{max}$ was 45, 55, and 50°, respectively, for compounds **1**−**3**. The space groups were determined from systematic absences and intensity statistics. The structures were solved by direct methods of SHELXS-86[23] and refined by full-matrix least-squares techniques of the TEXSAN[24] package of crystallography programs. Empirical absorption corrections based on ψ-scans were applied to all data sets, followed by a DIFABS[25] correction to the isotropically refined structure. The range of transmission factors following the ψ correction were as followes: **1**, 0.8184−1.000; **2**, 0.8301−1.000; **3**, 0.3839−1.000. All calculations were performed on a VAXstation 3100/76 computer. Complete data collection parameters and details of the structure solution

Table 1. Crystallographic Data for $[Ni(en)_3]Sb_2S_4$ (**1**), $[Co(en)_3]Sb_2S_4$ (**2**), and $[Ni(en)_3]Sb_4S_7$ (**3**)

	1	**2**	**3**
formula	$C_6H_{24}N_6NiS_4Sb_2$	$C_6H_{24}N_6CoS_4Sb_2$	$C_6H_{24}N_6NiS_7Sb_4$
fw	610.74	610.97	950.42
space group	$P2_1/c$	$P2_1/c$	$P2_1/c$
a,[a] Å	10.538(2)	21.131(4)	9.930(1)
b, Å	14.460(4)	14.619(2)	14.212(2)
c, Å	12.434(4)	12.540(2)	17.242(2)
β, deg	99.93(2)	100.50(1)	102.55(1)
Z; V, Å^3	4; 1866(2)	8; 3809(2)	4; 2375.1(9)
λ, Å	0.710 73	0.710 73	0.710 73
$d_{calc.}$, g/cm^3	2.173	2.131	2.658
μ (Mo Kα), cm^{-1}	43.27	41.16	59.07
T, °C	−120	−120	23
R/R_w,[b] %	6.0/7.2	5.4/10.3	2.9/4.0

[a] The lattice parameters reported are based on single crystal data. [b] $R = \sum||F_o| - |F_c||/\sum|F_o|$; $R_w = \{\sum w(|F_o| - |F_c|)^2/\sum w|F_o|^2\}^{1/2}$.

(22) (a) Wendlandt, W. W.; Hecht, H. G. *Reflectance Spectroscopy*; Interscience Publishers: New York, 1966. (b) Kortüm, G. *Reflectance Spectroscopy*; Springer Verlag: New York, 1969.
(23) Sheldrick, G. M. In *Crystallographic Computing 3*; Sheldrick, G. M., Krüger, C., Doddard, R., Eds.; Oxford University Press: Oxford, England, 1985; pp 175.
(24) *TEXSAN: Single Crystal Analysis Software*, Version 5.0; Molecular Structure Corp.: The Woodlands, TX , 1981.
(25) Walker, N.; Stuart, D. *Acta Crystallogr.* **1983**, *A39*, 158.

Table 2. Fractional Atomic Coordinates of the Non-Hydrogen Atoms and B_{eq} Values for $[Ni(en)_3]Sb_2S_4$ with Estimated Standard Deviations in Parentheses

atom	*x*	*y*	*z*	B_{eq},[a] Å^2
Sb(1)	0.71084(7)	0.28335(5)	−0.15118(8)	3.32(4)
Sb(2)	0.62143(6)	0.12726(5)	0.0675(6)	2.10(3)
Ni(1)	0.1783(1)	0.33512(8)	0.1621(1)	1.36(4)
S(1)	0.9177(2)	0.3457(2)	−0.1492(2)	2.0(1)
S(2)	0.7733(4)	0.1358(3)	−0.0604(5)	7.3(3)
S(3)	0.4317(3)	0.1690(2)	−0.0464(2)	2.6(1)
S(4)	0.6673(5)	0.2777(2)	0.1606(4)	7.2(2)
N(11)[b]	0.374(1)	0.350(1)	0.173(1)	1.7(3)
N(12)[b]	0.234(1)	0.354(1)	0.004(1)	1.7(3)
N(13)[b]	0.323(2)	0.444(1)	0.199(1)	2.1(3)
N(14)[b]	0.169(1)	0.438(1)	0.042(1)	1.8(3)
N(21)[b]	0.166(1)	0.435(1)	0.289(1)	1.6(3)
N(22)[b]	0.030(1)	0.431(1)	0.122(1)	1.6(3)
N(23)[b]	−0.030(1)	0.336(1)	0.157(1)	1.9(3)
N(24)[b]	0.135(1)	0.345(1)	0.317(1)	1.8(3)
N(31)[b]	0.056(1)	0.222(1)	0.112(1)	1.8(3)
N(32)[b]	0.154(1)	0.227(1)	0.048(1)	1.7(3)
N(33)[b]	0.318(1)	0.229(1)	0.200(1)	1.7(3)
N(34)[b]	0.203(1)	0.221(1)	0.276(1)	1.6(3)
C(11)	0.395(1)	0.4480(8)	0.113(1)	2.7(2)
C(12)	0.298(1)	0.4462(7)	0.008(1)	2.2(2)
C(21)	−0.054(1)	0.4255(8)	0.216(1)	2.6(2)
C(22)	0.050(1)	0.4286(7)	0.320(1)	2.2(2)
C(31)	0.241(1)	0.1402(7)	0.2099(9)	2.1(2)
C(32)	0.139(1)	0.1385(7)	0.108(1)	2.2(2)

[a] *B* values for anisotropically refined atoms are given in the form of the isotropic equivalent displacement parameter defined as $B_{eq} = (4/3)[a^2B(1,1) + b^2B(2,2) + c^2B(3,3) + ab(\cos\gamma)\,B(1,2) + ac(\cos\beta)\,B(1,3) + bc(\cos\alpha)\,B(2,3)$. [b] The site occupation factor is 0.5.

and refinement for compounds **1**−**3** are given in Table 1. The coordinates of all non-H atoms, average temperature factors and their estimated standard deviations are given in Tables 2−4.

Results and Discussion

Synthesis and Spectroscopy. The systematic investigation of hydrothermal reactions in the M^{2+}/Na_3SbS_3/en system within the ratio range of 1.0/0.5−5.0/3−36 yielded six new compounds. The synthetic conditions under which compounds **1**−**4** as well as $[Co(en)_3]CoSb_4S_8$[19] and $[Fe(en)_3]Sb_2S_4$[26] are formed are summarized in Table 5. The formation of SbS_2^- and $Sb_4S_7^{2-}$ chains, respectively, is the result of condensation processes of the SbS_3^{3-} ligand according to the following equations:

$$n\mathrm{H_2O} + n\mathrm{SbS_3^{3-}} \rightarrow (1/n)[\mathrm{SbS_2}]^- + n\mathrm{HS^-} + n\mathrm{OH^-} \quad (1)$$

$$5n\mathrm{H_2O} + 4n\mathrm{SbS_3^{3-}} \rightarrow (1/n)[\mathrm{Sb_4S_7}]^{2-} + 5n\mathrm{HS^-} + 5n\mathrm{OH^-} \quad (2)$$

Except for $[Co(en)_3]CoSb_4S_8$, there is no evidence for metal/antimony/sulfide frameworks. Instead, the negative charges of the antimony sulfide chains are balanced by tris(ethylenediamine)metal(II) complexes which form *in situ*. It is interesting to note that the formation of the simple SbS^{2-} chains is favored if the en content is relatively high, while the more complicated $Sb_4S_7^{2-}$ chain forms at lower en ratios (see Table 5). A reasonable explanation for this observation might be that the antimony sulfide species present in the reaction mixtures undergo hydrolysis. In particular, the possible equilibrium in eq 3 would favor the formation of simple SbS_2^- chains for comparably high pH values and low water contents which is clearly the case for all three $[M(en)_3]Sb_2S_4$ compounds (see Table 5).

$$4\mathrm{SbS_2^-} + \mathrm{H_2O} \rightarrow \mathrm{Sb_4S_7^{2-}} + \mathrm{HS^-} + \mathrm{OH^-} \quad (3)$$

The ethylenediamine metal complexes form *in situ* under the conditions of our experiments and they act as counterions for the anionic frameworks. Although the original discovery of such complexes in these reactions was unanticipated, since the intent was to incorporate the transition metals into the anionic framework, it is now clear that the very high stability constants of $[M(en)_3]^{2+}$ were underestimated as a driving force. Nevertheless, given these facts, the deliberate use of $[M(en)_3]^{2+}$ as charge balancing species could prove beneficial because they could stabilize different frameworks from those observed with the more conventional R_4N^+ cations. Other examples of compounds in which these metals complexes occur as counterions include $[Fe(en)_3]_2(Hg_2Te_9)$,[26] $[M(en)_3]In_2Te_6$ (M = Fe, Zn),[27] and $[La(en)_4Cl]In_2Te_4$.[28]

In all of these reactions we observed substantial amounts of black fluffy powder, which according to EDS and XRD analyses

Table 3. Fractional Atomic Coordinates of the Non-Hydrogen Atoms and B_{eq} Values for $[Co(en)_3]Sb_2S_4$ with Estimated Standard Deviations in Parentheses

atom	*x*	*y*	*z*	B_{eq},[a] Å^2
Sb(1)	0.14331(9)	0.2220(1)	0.1700(1)	1.48(7)
Sb(2)	0.1876(1)	0.1252(1)	0.4455(1)	1.43(7)
Sb(3)	0.64436(8)	0.2098(1)	0.1345(1)	1.25(7)
Sb(4)	0.68948(9)	0.1310(1)	0.4217(1)	1.22(7)
Co(1)	0.0924(2)	0.8356(3)	0.1606(3)	1.3(1)
Co(2)	0.5883(2)	0.8334(3)	0.1655(3)	1.0(1)
S(1)	0.1213(3)	0.3745(5)	0.0883(6)	1.7(3)
S(2)	0.1540(4)	0.2765(5)	0.3607(6)	1.9(3)
S(3)	0.0380(4)	0.1608(5)	0.1451(6)	1.9(3)
S(4)	0.2873(4)	0.1665(7)	0.5451(7)	3.0(4)
S(5)	0.6053(3)	0.3503(5)	0.0347(5)	1.4(1)
S(6)	0.6760(3)	0.2782(5)	0.3184(5)	1.6(3)
S(7)	0.5424(3)	0.1479(5)	0.1499(5)	1.5(3)
S(8)	0.7800(3)	0.1729(6)	0.5494(6)	2.0(3)
N(1)	0.161(1)	0.725(2)	0.203(2)	2.3(5)
N(2)	0.029(1)	0.720(2)	0.116(2)	2.1(4)
N(3)	0.065(1)	0.846(2)	0.319(2)	1.6(4)
N(4)	0.015(1)	0.932(2)	0.124(2)	1.3(4)
N(5)	0.165(1)	0.945(2)	0.199(2)	1.9(4)
N(6)	0.122(1)	0.854(2)	0.004(2)	1.8(4)
N(7)	0.688(1)	0.851(2)	0.174(2)	1.8(4)
N(8)	0.589(1)	0.938(2)	0.044(2)	2.2(5)
N(9)	0.583(1)	0.935(2)	0.291(2)	1.7(4)
N(10)	0.486(1)	0.835(2)	0.157(2)	1.7(4)
N(11)	0.605(1)	0.717(2)	0.277(2)	1.2(4)
N(12)	0.579(1)	0.723(2)	0.050(2)	1.4(4)
C(1)	0.123(1)	0.639(2)	0.203(2)	1.7(5)
C(2)	0.070(1)	0.637(2)	0.112(2)	1.7(5)
C(3)	0.030(1)	0.930(2)	0.321(2)	1.1(4)
C(4)	−0.024(1)	0.934(2)	0.216(2)	1.4(5)
C(5)	0.197(1)	0.959(2)	0.106(2)	2.1(5)
C(6)	0.149(1)	0.946(2)	−0.000(2)	1.7(5)
C(7)	0.701(1)	0.940(2)	0.123(2)	1.7(5)
C(8)	0.652(2)	0.951(2)	0.017(2)	2.4(6)
C(9)	0.514(1)	0.927(2)	0.317(2)	1.7(5)
C(10)	0.469(2)	0.916(2)	0.215(3)	2.8(6)
C(11)	0.619(1)	0.635(2)	0.213(2)	1.7(5)
C(12)	0.569(1)	0.636(2)	0.102(2)	2.2(5)

[a] *B* values for anisotropically refined atoms are given in the form of the isotropic equivalent displacement parameter defined as $B_{eq} = (4/3)[a^2B(1,1) + b^2B(2,2) + c^2B(3,3) + ab(\cos\gamma)\,B(1,2) + ac(\cos\beta)\,B(1,3) + bc(\cos\alpha)\,B(2,3)$.

(26) $[Fe(en)_3]Sb_2S_4$ can be isolated as a trace (estimated yield << 1%). The main product is a black powder and red crystals of Sb_2S_3.

(27) Li, J.; Rafferty, B. G.; Mulley, S.; Proserpio, D. M. *Inorg. Chem.* **1995**, *34*, 6417.

(28) Li, J.; Chen, Z.; Emge, T. J.; Proserpio, D. M. *Inorg. Chem.* **1997**, *36*, 20.

(29) Li, J.; Chen, Z.; Chen, F.; Proserpio, D. M. *Inorg. Chim. Acta*., in press.

Table 4. Fractional Atomic Coordinates of the Non-Hydrogen Atoms and B_{eq} Values for $[Ni(en)_3]Sb_4S_7$ with Estimated Standard Deviations in Parentheses

atom	*x*	*y*	*z*	B_{eq},[a] Å^2
Sb(1)	0.45803(5)	0.35623(4)	0.01176(3)	1.95(2)
Sb(2)	0.51548(5)	0.10869(4)	0.09311(3)	1.65(2)
Sb(3)	0.50254(5)	−0.13883(4)	0.15886(3)	1.83(2)
Sb(4)	0.51172(5)	0.04280(4)	0.31835(3)	1.70(2)
Ni(1)	−0.00487(9)	0.24044(7)	0.18208(6)	1.72(4)
S(1)	0.3188(2)	0.4147(2)	−0.1155(1)	2.28(8)
S(2)	0.6608(2)	0.3184(2)	−0.0287(1)	3.1(1)
S(3)	0.3358(2)	0.2007(1)	−0.0008(1)	2.24(8)
S(4)	0.3680(2)	−0.0285(1)	0.0579(1)	1.94(7)
S(5)	0.4354(2)	0.1629(1)	0.2139(1)	2.05(8)
S(6)	0.6894(2)	−0.0324(1)	0.2072(1)	2.20(8)
S(7)	0.3676(2)	−0.0914(1)	0.2589(1)	2.31(8)
N(1)	−0.1044(6)	0.3703(5)	0.1457(4)	2.5(3)
N(2)	0.1520(6)	0.3059(5)	0.1330(4)	2.4(3)
N(3)	−0.0998(7)	0.1769(5)	0.0728(5)	3.0(3)
N(4)	0.0961(6)	0.1071(5)	0.1979(4)	2.4(3)
N(5)	−0.1638(6)	0.1951(5)	0.2409(5)	2.5(3)
N(6)	0.0875(6)	0.2814(5)	0.3003(4)	2.1(3)
C(1)	−0.0061(8)	0.4357(6)	0.1224(6)	2.9(4)
C(2)	0.090(1)	0.3843(7)	0.0818(6)	3.4(4)
C(3)	−0.019(1)	0.0936(7)	0.0600(6)	3.7(4)
C(4)	0.031(1)	0.0431(6)	0.1336(6)	3.4(4)
C(5)	−0.107(1)	0.1943(7)	0.3266(6)	3.5(4)
C(6)	−0.018(1)	0.2778(7)	0.3486(6)	3.4(4)

[a] *B* values for anisotropically refined atoms are given in the form of the isotropic equivalent displacement parameter defined as $B_{eq} = (4/3)[a^2B(1,1) + b^2B(2,2) + c^2B(3,3) + ab(\cos\gamma)B(1,2) + ac(\cos\beta)B(1,3) + bc(\cos\alpha)\,B(2,3)$.

Table 5. Reagent Stoichiometric Mole Ratios for the Syntheses of Compounds **1**−**4**, $[Co(en)_3]CoSb_4S_8$, and $[Fe(en)_3]Sb_2S_4$

	$M(Hal)_2$	Na_3SbS_3	en	H_2O
$[Ni(en)_3]Sb_2S_4$ (**1**)	1	2	12	120
$[Co(en)_3]Sb_2S_4$ (**2**)	1	0.8	36	30
$[Ni(en)_3]Sb_4S_7$ (**3**)	1	1.5	6	140
$[Fe(en)_3]Sb_4S_7$	1	1.1	12	120
$[Co(en)_3]CoSb_4S_8$[19] (**4**)	1	0.8	12	120
$[Fe(en)_3]Sb_2S_4$[26]	1	0.8	36	30

consists of mixtures of $NaSbS_2$ and Sb_2S_3. This powder is the main product if the ratio of M^{2+}/SbS_3^{3-} of 1/1.5 (M = Fe, Co) or 1/2.5 (M = Ni) is exceeded. However, it is possible to remove this powder mechanically by sonicating the reaction products in solvents such as water or acetone and subsequently decanting the liquid. Frequently, even highly crystalline samples contain black impurities trapped inside the crystals. These impurities make the powder look slightly grayish and thus have a visible impact on the optical properites of the bulk ground samples.

The IR spectroscopic data given for compounds **1**-**4** are complex and can serve as "fingerprints". However, the absorbances between 525 and 475 cm^{-1} can be assigned to M−N vibration modes arising from the $[M(en)_3]^{2+}$ cations, since $[Ni(en)_3]Cl_2$ shows two strong absorbances in the same region (524 and 499 cm^{-1}). All other signals arise from Sb−S vibrations.

The optical properties have been studied by single-crystal UV/vis spectroscopy (compounds **1**−**3**) and UV/near-IR reflectance spectroscopy (compounds **1**−**4**). The single crystal spectra are depicted in Figure 1, the reflectance spectra, in Figure 2. The spectra confirm that these valence-precise materials are wide-band gap semiconductors with sharp optical gaps attributed to excitations from filled S-based orbitals to Sb-based empty orbitals. The single crystal spectra of the nickel compounds **1** and **3** show absorbances aring from both the $[Ni(en)_3]^{2+}$ cations (d−d transitions) and the Sb/S frameworks (band gap). The estimated band gaps are 2.49 (**1**) and 2.62 eV (**3**). In addition,

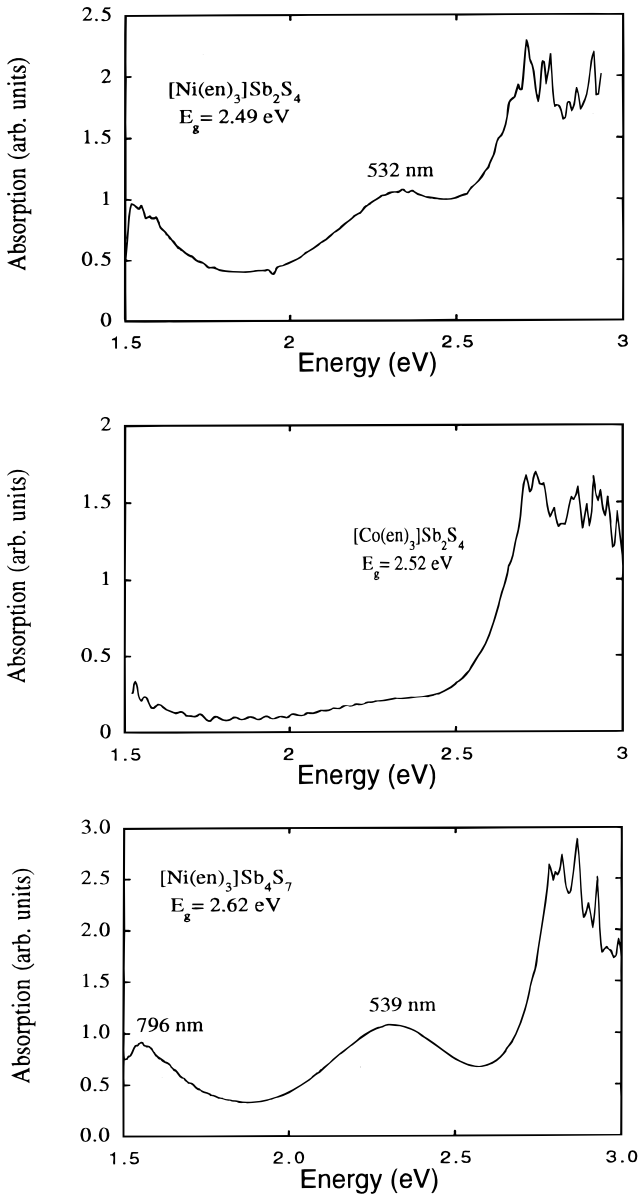

Figure 1. Single crystal absorption spectra for compounds **1** (A, top), **2** (B, middle), and **3** (C, bottom).

one of the three spin allowed transitions in the $[Ni(en)_3]^{2+}$ complexes is observed around 540 nm ($^3T_{1g}$ (F) ← $^3A_{2g}$) in both nickel compounds. The low-energy transition[30] $^3T_{2g}$ ← $^3A_{2g}$ (expected at 910 nm) is beyond the reach of our equipment; however, it is observed as a weak transition in the diffuse reflectance spectrum (see below). The high-energy transition[31] $^3T_{1g}$ (P) ← $^3A_{2g}$ expected at 330 nm is masked by the strong charge transfer transition from $S^{2-} \rightarrow Sb^{3+}$.

From the diffuse reflectance spectra of compounds **1** and **3**, band gaps of 2.72 (**1**) and 2.35 eV (**3**) can be assessed. In these spectra, the weak absorbances at ∼1.4 eV can be assigned to the $^3T_{2g}$ ← $^3A_{2g}$ transitions, while the absorbance oberserved in the single crystal experiment at 540 nm is hidden under the onset of the band gap absorption. The difference in the optical data obtained from the powdered samples compared with the single crystal samples of compounds **1** and **3** might be due to the broader nature and lower resolution of the powder spectra.

(30) Cotton, F. A.; Wilkinson, G. *Advanced Inorganic Chemistry*, 5th ed.; John Wiley & Sons: New York, Chichester, Brisbane, Toronto, Singapore, 1988; p 744.
(31) Lever, A. B. P. *Inorganic Electronic Spectroscopy*, 2nd ed.; Elsevier: Amsterdam, Oxford, New York, Tokyo, 1984.

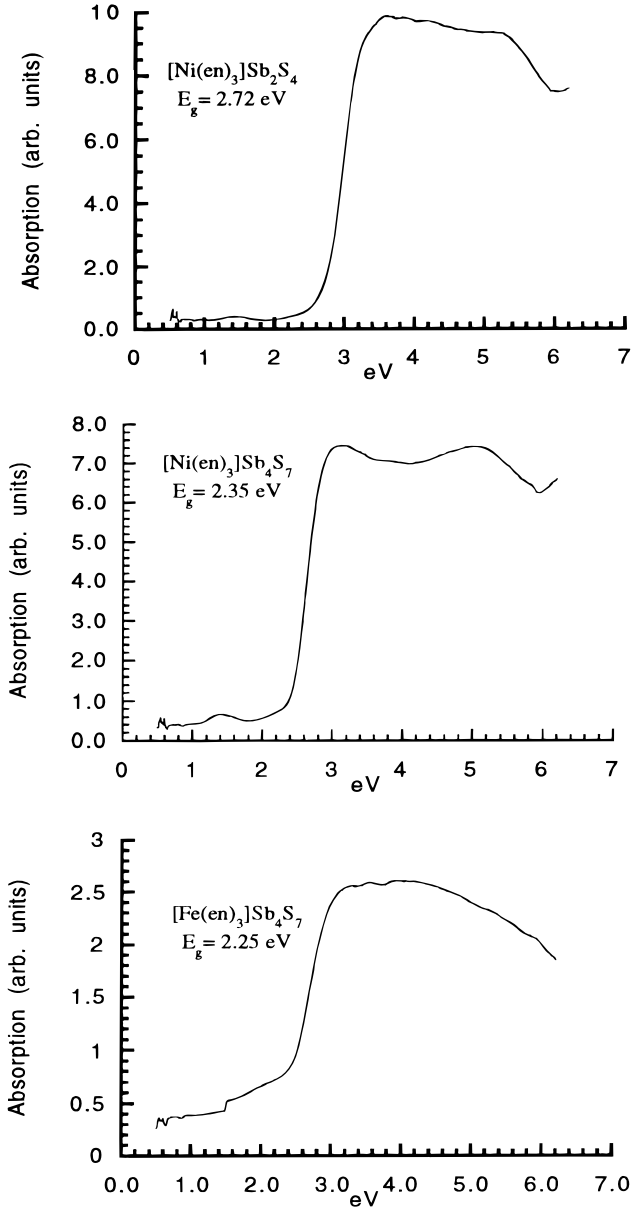

Figure 2. Diffuse reflectance spectra for compound **1** (A, top), **3** (B, middle), and **4** (C, bottom).

However, the single crystal absorption spectrum of compound **2** reveals a band gap of 2.52 eV which compares well with that of compound **1** (2.49 eV). For compound **2**, no d−d transitions could be observed since they are 2 orders in magnitude less intense compared with the nickel compounds.[31] The same is true for compound **4** for which a band gap of 2.25 eV was estimated from the diffuse reflectance spectrum.

Structure of $[Ni(en)_3]Sb_2S_4$ (1) and $[Co(en)_3]Sb_2S_4$ (2). The crystal structures of compound **1** and **2** consist of isolated $[M(en)_3]^{2+}$ complexes and infinite $1/\infty[SbS_2]^-$ chains, which are shown in Figure 3. These chains are built by pyramidal SbS_3 units that are connected via corners. As a result, each SbS_3 unit has two bridging and one terminal S atoms. The Sb−S bond distances range from 2.325(3) to 2.470(4) Å (**1**) and from 2.329(9) to 2.501(7) Å (**2**) with mean values of 2.420 (**1**) and 2.439 Å (**2**). As expected, the Sb−S(terminal) bond lengthes (2.340 Å for **1**; 2.353 Å for **2**) are about 0.12 Å shorter than the Sb−S(bridging) bonds (2.460 Å for **1**; 2.483 Å for **2**). The S−Sb−S angles (range for **1**, 96.7(1)−100.3(1)°; range for **2**, 95.0(3)−100.9(3)°) are typical for pyramidal SbS_3 units and demonstrate clearly the presence of stereochemically active lone pairs. There is no evidence for any significant secondary Sb···S interactions. The shortest Sb···S contact is 3.70 Å long (Sb(3)···S(8′) in compound **2**. Selected bond distances and angles for both compounds **1** and **2** are given in Table 6.

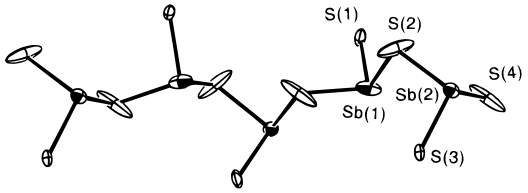

Figure 3. $[Ni(en)_3]Sb_2S_4$: ORTEP representation of the SbS^{2-} chain (50% probability ellispoids).

Table 6. Selected Distances (Å) and Angles (deg) for $[Ni(en)_3]Sb_2S_4$ and $[Co(en)_3]Sb_2S_4$ with Standard Deviations in Parentheses

	$[Ni(en)_3]Sb_2S_4$		
Sb(2)−S(2)	2.450(4)	S(2)−Sb(2)−S(3)	100.2(1)
Sb(2)−S(3)	2.325(3)	S(2)−Sb(2)−S(4)	99.3(2)
Sb(2)−S(4)	2.470(4)	S(3)−Sb(2)−S(4)	97.8(1)
Sb(1)−S(1)	2.355(3)	S(1)−Sb(1)−S(2)	98.8(1)
Sb(1)−S(2)	2.450(3)	S(1)−Sb(1)−S(4)	99.6(2)
Sb(1)−S(4)	2.470(5)	S(2)−Sb(1)−S(4)	96.7(2)
	$[Co(en)_3]Sb_2S_4$		
Sb(1)−S(1)	2.463(8)	S(1)−Sb(1)−S(2)	95.0(3)
Sb(1)−S(2)	2.492(7)	S(1)−Sb(1)−S(3)	100.7(3)
Sb(1)−S(3)	2.366(8)	S(2)−Sb(1)−S(3)	99.6(2)
Sb(2)−S(1)	2.467(7)	S(1)−Sb(2)−S(2)	98.8(3)
Sb(2)−S(2)	2.500(8)	S(1)−Sb(2)−S(4)	100.9(3)
Sb(2)−S(4)	2.325(9)	S(2)−Sb(2)−S(4)	99.1(3)
Sb(3)−S(5)	2.466(7)	S(5)−Sb(3)−S(7)	97.7(2)
Sb(3)−S(7)	2.377(7)	S(5)−Sb(3)−S(6)	98.3(2)
Sb(3)−S(6)	2.491(7)	S(7)−Sb(3)−S(6)	99.9(2)
Sb(4)−S(8)	2.342(7)	S(8)−Sb(4)−S(5)	99.3(2)
Sb(4)−S(5)	2.483(7)	S(8)−Sb(4)−S(6)	97.5(3)
Sb(4)−S(6)	2.501(7)	S(5)−Sb(4)−S(6)	100.1(2)

SbS^{2-} chains, as structural features of Sb^{3+}/S compounds, have been reported for both minerals (e.g., wolfbergite $CuSbS_2$,[32] berthierite $FeSb_2S_4$,[33] and livingstonite $HgSb_4S_8$[34]) and synthetic compounds such as $Cs_3Ag_2Sb_3S_8$[12] ($Sb^{3+}S_2$ chains besides $Sb^{5+}S_4$ tetrahedra) and $[Co(en)_3]CoSb_4S_8$[19] in which the terminal sulfur atoms of the SbS_2 chains act as ligands for the tetrahedral cobalt sites resulting in microporous $[CoSb_4S_8]^{2-}$ layers.

Chains of corner-sharing pyramids are also known for As^{3+} ($AASe_2$,[35] A = K, Rb, Cs) and Bi^{3+} ($[Et_4N]BiSe_2$[36]) as well as for the antimony selenide compound $[Ba(en)_4]Sb_2Se_4$.[37] In general, Sb^{3+} chalcogenide compounds can adopt coordination numbers of 3, 4, 5, or 6.[1−15] However, the formation of pyramidal SbS_3 units in compounds **1** and **2** might be caused by the cation-size effect: The connectivity/dimensionality of the anionic framework is generally reduced in the presence of large cations.[38] For instance, the compound β-$NaSbS_2$[1a] (small Na^+ ions) possesses a three-dimensional cubic structure of the NaCl type with octahedral SbS_6 units, while the larger Cs cation favors the formation of a two-dimensional Sb/S and one

(32) Wernick, J. H.; Benson, K. E. *J. Phys. Chem. Solids* **1957**, *3*, 157.
(33) Buerger, M. J.; Hahn, T. *Am. Mineral* **1955**, *40*, 226.
(34) Buerger, M. J.; Niizeki, N. *Z. Krystallogr.* **1957**, *109*, 129.
(35) Sheldrick, W. S.; Häusler, H.-J. *Z. Anorg. Allg. Chem.* **1988**, *561*, 139.
(36) Pell, M. A.; Ibers, J. A. *Inorg. Chem.* **1996**, *35*, 4559.
(37) König, T.; Eisenmann, B.; Schäfer, H. *Z. Anorg. Allg. Chem.* **1982**, *488*, 126.
(38) Kanatzidis, M. G. *Phosphorous, Sulfur Silicon Relat. Elements* **1994**, *93*−*94*, 159.
(39) McCarthy, T. J.; Ngeyi, S.-P.; Liao, J.-H.; DeGroot, D.; Hogan, T.; Kannewurf, C. R.; Kanatzidis, M. G. *Chem. Mater.* **1993**, *5*, 331.

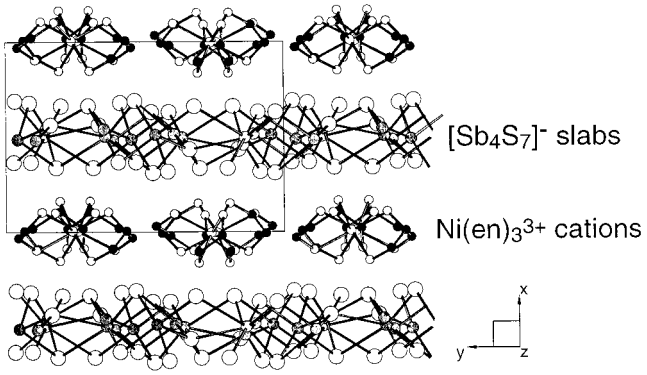

Figure 4. Unit cell of $[Ni(en)_3]Sb_4S_7$. The separation of anions and cations into layers is evident.

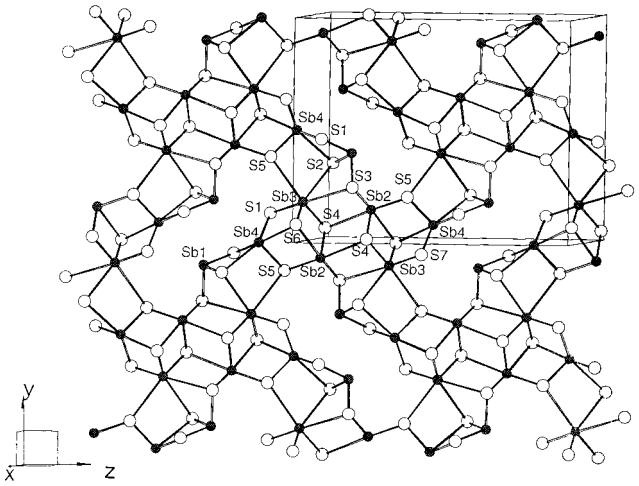

Figure 5. $[Ni(en)_3]Sb_4S_7$: The $Sb_4S_7^{2-}$ slab.

dimensional framework of $[SbS_2]^-$.[39] Consequently, materials with lower dimensionalities may form in the presence of larger $[M(en)_3]^{2+}$ cations as observed in compounds **1** and **2**.

The ethylenediamine ligands of the $[Ni(en)_3]^{2+}$ cations in **1** are disordered so that it is very diffuclt to determine the conformation of these complexes in crystals of compound **1**. However, the crystal lattice of compound **2** is a superstructure of the lattice of compound **1** since the *a*-axis is doubled. As a result, the $[Co(en)_3]^{2+}$ cations are ordered with two symmetry independent cations in the asymmetric unit. Both cations exhibit either the $\Delta(\lambda\lambda\lambda)$ or $\Lambda(\delta\delta\delta)$ conformation. The M−N distances and N−M−N bond angles of compounds **1** and **2** are normal and call for no further comment. A similar superstructure was not evident in axial rotation photographs of compound **1**.

Structure of $[Ni(en)_3]Sb_4S_7$. The anions and the cations in this compound are segregated along the *a*-axis into layers; see Figure 4. The anionic part of the structure represents a transition state between a one-dimensional and two-dimensional framework; see Figure 5. Each $[Sb_4S_7]^{2-}$ slab is made from the side-by-side association of clearly recognizable infinite one-dimensional $[Sb_4S_7]^{2-}$ chains which run along the crystallographic *c*-axis; see Figure 6. Each chain is composed of pyramidal (Ψ-tetrahedral) SbS_3 units. Three of those units corner-share to form Sb_3S_6 six-membered rings in chair conformation. The infinite zigzag $[Sb_4S_7]^{2-}$ chains then form via a connection to a fourth SbS_3 unit. Again, the $Sb-S_t$ distances are ca. 0.12 Å shorter than the $Sb-S_b$ distances. The mean Sb−S distance is 2.467 Å; the mean S−Sb−S angle is 94.6°.

A more detailed investigation of the structural data reveals that each of the four symmetry independent Sb atoms has a different secondary coordination sphere (Figure 7). While

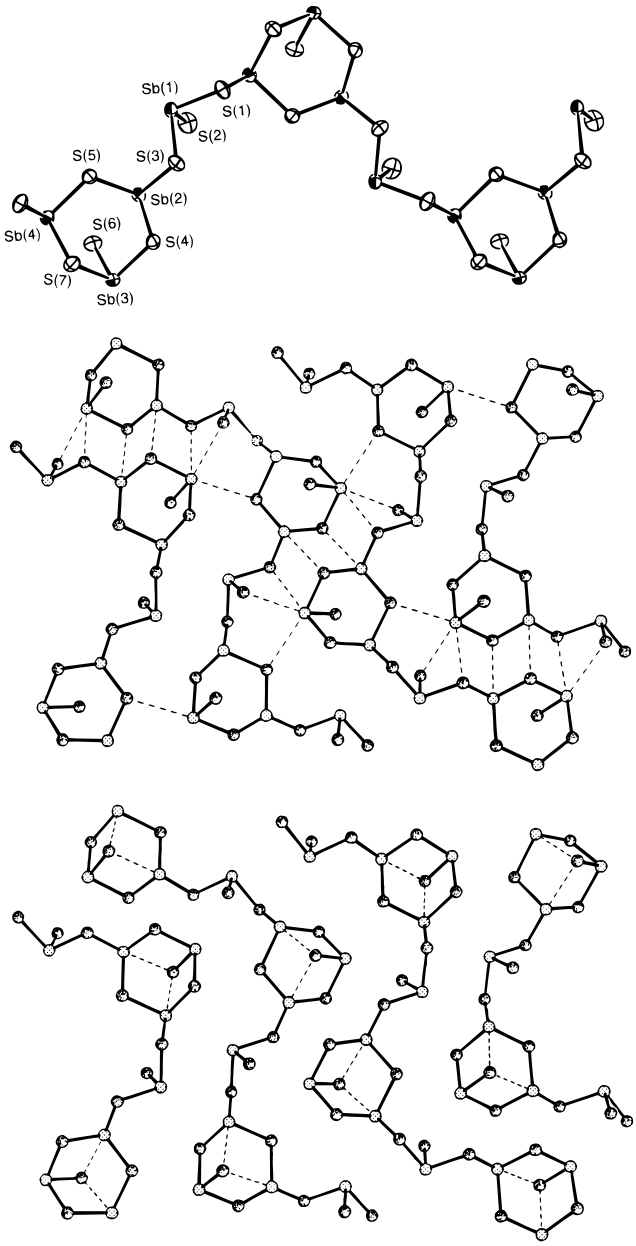

Figure 6. $[Ni(en)_3]Sb_4S_7$: (A, top) ORTEP representation of a portion of the $Sb_4S_7^{2-}$ chain (50% probability ellispoids), (B, middle) adjacent $Sb_4S_7^{2-}$ chains with intermolecular contacts, and (C, bottom) intramolecular contacts within a chain.

Sb(1)) only has van der Waals contacts to the sulfur atoms in its second coordination sphere (Sb···S > 4.0 Å) and thus is in a true pyramidal (3 + 0) coordination, Sb(4) shows a (3 + 1) coordination with a fourth Sb···S distance of 3.066 Å to S(6). The geometry of this SbS_4 unit is similar to the sphenoid structure of SF_4. Sb(2) shows the same weak contact with the intracyclic S(6) atom (Sb(2)···S(6) = 3.066 Å) and an additional intermolecular contact with S(4′) of 3.275 Å. The geometry of this (3 + 2) coordinated Sb(2) is square pyramidal. Sb(3) is in a distorted octahedral (3 + 3) coordination with three additonal intermolecular contacts with S(2′) (3.55 Å), S(3′) (3.56 Å), and S(5′) (3.542 Å). The contacts between the $Sb_4S_7^{2-}$ create a pseudo-two-dimensional network which is shown in Figure 6A. The infinite $1/\infty[Sb_4S_7]^{2-}$ chains described here are not very common for Sb^{3+}/S compounds but have been reported for $[pipH_2]Sb_4S_7$[14] (pip = 2-[[[2-(2-pyridyl)ethyl]imino]ethyl]pyridine) and $[NH_4]_2Sb_4S_7$.[40] We note, however, the mode and

(40) Dittmar, G.; Schäfer, H. *Z. Anorg. Allg. Chem.* **1977**, *437*, 183.

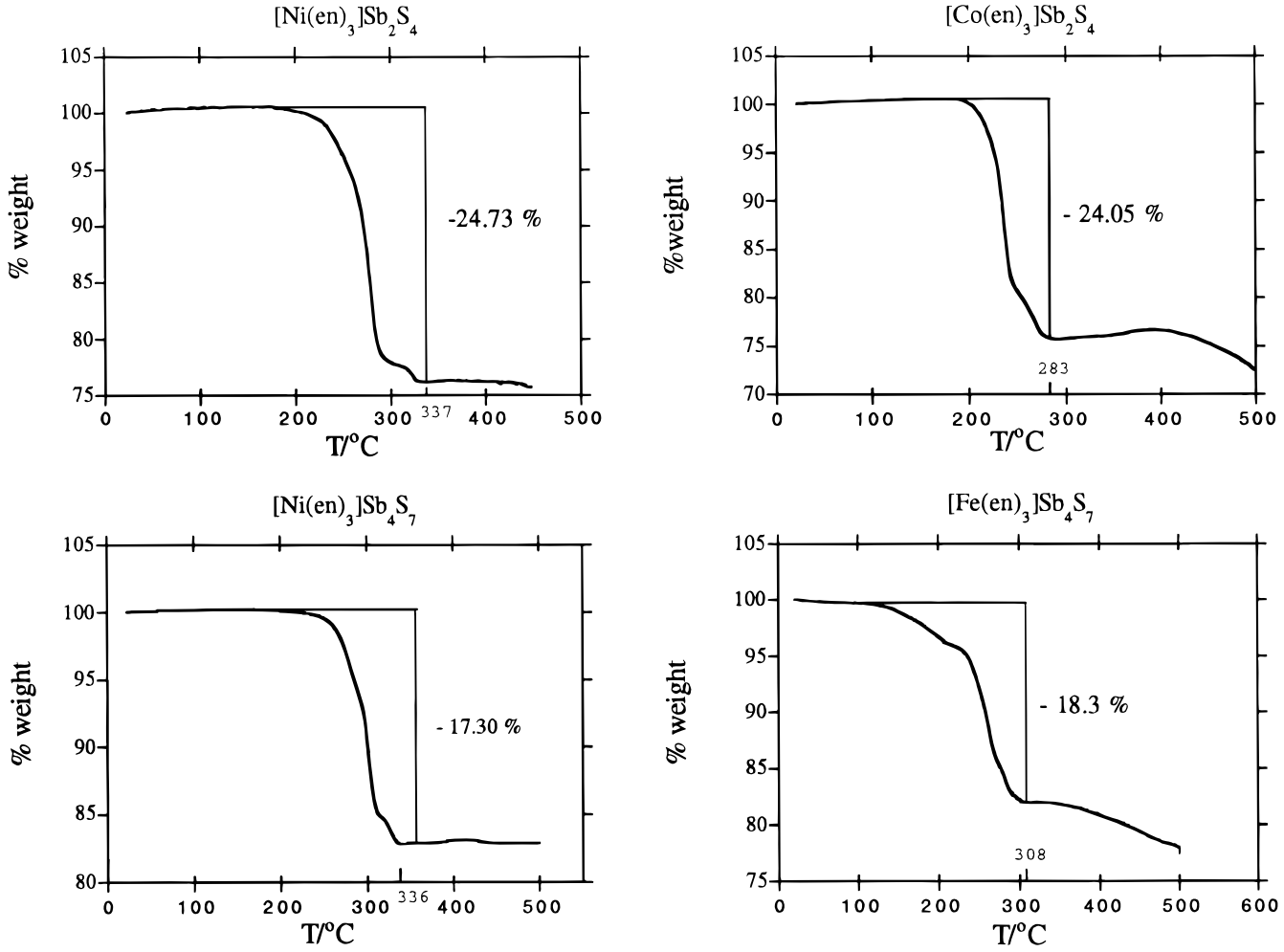

Figure 7. Thermogravimetric analyses of compounds **1** (A, top right), **2** (B, top right), **3** (C, bottom left) and **4** (D, bottom right).

Table 7. Selected Distances (Å) and Angles (deg) for $[Ni(en)_3]Sb_4S_7$ with Standard Deviations in Parentheses

Sb(1)−S(1)	2.470(2)	Sb(3)−S(4)	2.502(2)
Sb(1)−S(2)	2.332(2)	Sb(3)−S(6)	2.399(2)
Sb(1)−S(3)	2.509(2)	Sb(3)−S(7)	2.496(2)
Sb(2)−S(3)	2.502(2)	Sb(4)−S(1)	2.507(2)
Sb(2)−S(4)	2.434(2)	Sb(4)−S(5)	2.477(2)
Sb(2)−S(5)	2.508(2)	Sb(4)−S(7)	2.470(2)
	Long Interactions		
Sb(2)−S(4′)	3.276(2)	Sb(3)−S(5′)	3.541(2)
Sb(2)−S(6′)	3.065(2)	Sb(4)−S(2′)	3.367(3)
Sb(3)−S(2′)	3.549(3)	Sb(4)−S(6′)	3.066(2)
Sb(3)−S(3′)	3.561(2)		
S(1)−Sb(1)−S(2)	99.48(8)	S(4)−Sb(3)−S(7)	91.47(7)
S(1)−Sb(1)−S(3)	93.03(7)	S(6)−Sb(3)−S(7)	94.63(7)
Sb(1)−S(1)−Sb(4)	98.60(7)	S(1)−Sb(4)−S(5)	91.20(7)
S(2)−Sb(1)−S(3)	101.78(8)	S(1)−Sb(4)−S(7)	86.78(7)
S(3)−Sb(2)−S(4)	87.21(7)	Sb(2)−S(4)−Sb(3)	97.32(7)
S(3)−Sb(2)−S(5)	93.82(7)	S(5)−Sb(4)−S(7)	99.93(7)
S(4)−Sb(2)−S(5)	99.84(7)	Sb(2)−S(5)−Sb(4)	106.84(7)
Sb(1)−S(3)−Sb(2)	98.10(7)	Sb(3)−S(7)−Sb(4)	98.38(7)
S(4)−Sb(3)−S(6)	95.84(7)		

degrees of association of these chains are different in all three compounds. Selected bond distances and angles for compound **3** are given in Table 7.

In contrast to the $[M(en)_3]^{2+}$ cations in compounds **1** and **2**, $[Ni(en)_3]^{2+}$ in compound **3** show $\Delta(\lambda\lambda\lambda)$ and $\Lambda(\delta\delta\delta)$ conformations. The average Ni−N distance is 2.15 Å long and thus is within the normal range.

Thermogravimetric Analyses. The results of the thermogravimetric analyses performed between 20 and 500 °C are shown in Figure 7. The observed weight losses of 25.6 (**1**), 24.9 (**2**), 17.3 (**3**), and 17.7% (**4**) are in accordance with the complete loss of ethylenediamine (theoretical values: 29.5% for compounda **1** and **2** and 19.0% for compounds **3** and **4**). The shape or the curves, in particular the curve of compound **4**, suggests that the decomposition of compounds **1**−**4** is possibly a multistep rather than a one-step process since none of the curves shows a clean one-step loss of ethylenediamine. This behavior suggested that novel ternary metal/antimony/sulfide phases may form during the decompositon process. For that reason, we recorded the powder diffraction patterns of samples of compounds **1**−**4** that were heated to 300 °C. At this temperature, the weight loss was complete for all compounds. Unfortunately, all of the powder diffraction patterns showed lines that could only be assigned to Sb_2S_3. Obviously, the decomposition is associated with phase separation, leading to the binary sulfide Sb_2S_3 and amorphous M/S phases which did not appear in the powder pattern. This behavior was also observed for $[Co(en)_3]CoSb_4S_8$.[19]

Magnetic Data. The temperature dependent susceptibility data for compounds **1**−**4** were recorded in the temperature range from 2 to 300 K. All compounds contain high-spin paramagnetic tris(ethylenediamine)metal(II) complexes which obey Curie−Weiss law between 100 and 300 K. The susceptibility plots for compound **1**−**4** are depicted in Figure 8. The

(41) Boudreaux, E. A.; Mulay, L. N. *Theory and Applications of Molecular Paramagnetism*; John Wiley & Sons: New York, London, Sydney, Toronto, 1976.
(42) Bensch W.; Schur, M. *Z. Naturforsch.* **1997**, *52B*, 405.

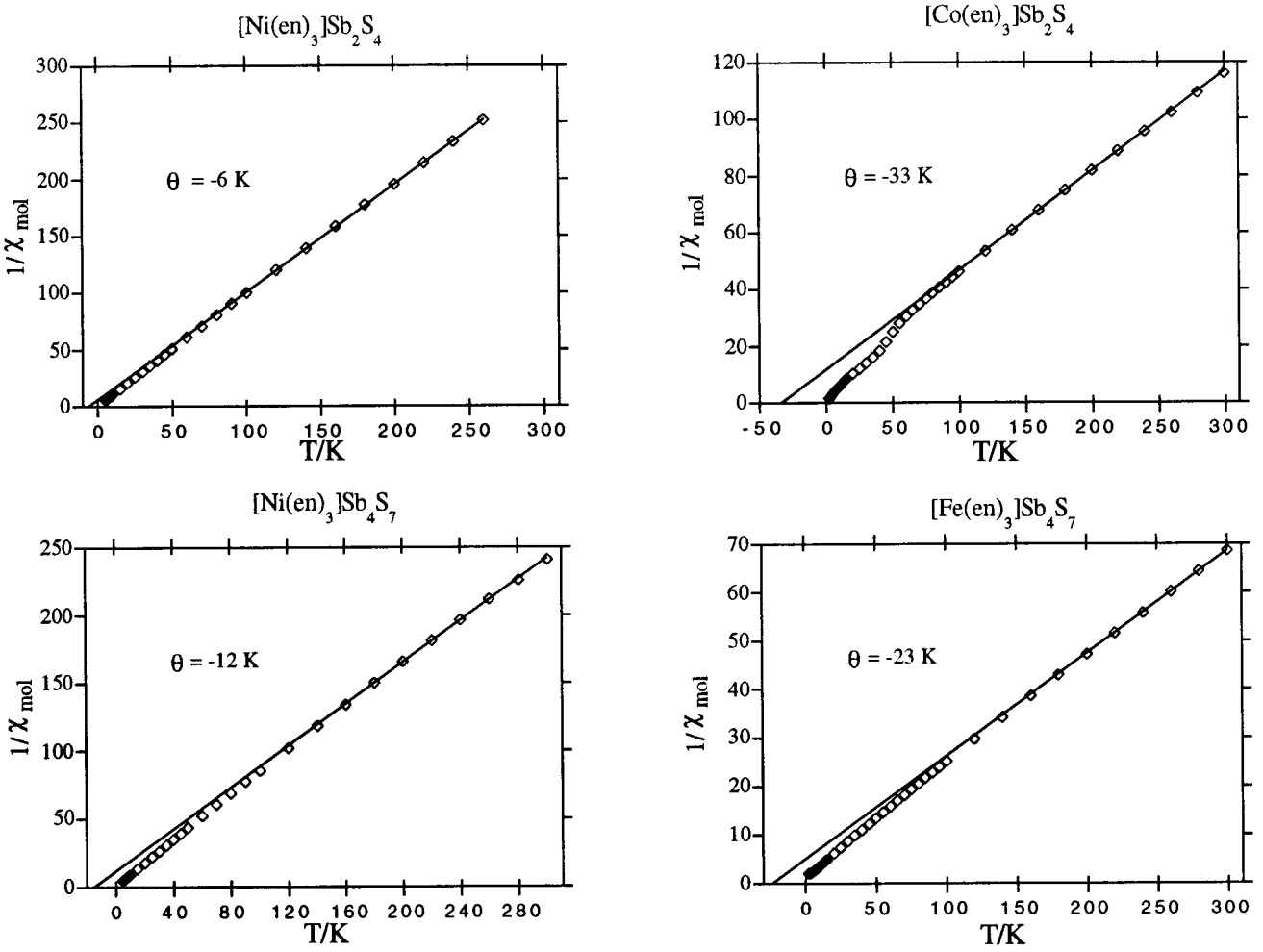

Figure 8. Variable temperature magnetic susceptibility data for compounds **1** (A, top left), **2** (B, top right), **3** (C, bottom left) and **4** (D, bottom right).

calculated effective moments at room temperature are 3.10 (**1**), 4.57 (**2**), 3.16 (**3**), and 5.94 μ_B (**4**). For comparison, octahedral Ni(II) complexes usually show effective moments between 2.76 and 3.40 μ_B, while octahedrally coordinated Co(II) and Fe(II) compounds have moments of 4.7−5.1 μ_B and 5.2−5.6 μ_B.[41] At temperatures below 100 K, significant deviations from the Curie−Weiss law are observed. The Weiss constants are −6 (**1**), −33 (**2**), −12 (**3**), and −23 K (**4**). While this manuscript was being revised, the isostructural Mn analogue of compound **3** was reported.[42]

Acknowledgment. Financial support from the donors of the Petroleum Research Fund, administered by the American Chemical Society, is gratefully acknowledged. H.-O.S. thanks the Deutsche Forschungsgemeinschaft for a postdoctoral research fellowship.

Supporting Information Available: Tables of atomic coordinates of all atoms, anisotropic thermal parameters, bond distances and angles, and crysstallographic data for compounds **1**−**3** (32 pages). Ordering information is given on any current masthead page.

IC970609+